

Transition from classical to ultimate melting

Edoardo Bellincioni^{1*†}, Kevin Zhong^{1*†},
 Christopher J. Howland², Yiyu Zhou⁵, Sander G. Huisman¹,
 Roberto Verzicco^{1,3}, Detlef Lohse^{1,4*}

¹Physics of Fluids Department and Max Planck Center for Complex Fluid Dynamics and J. M. Burgers Centre for Fluid Dynamics, University of Twente, P. O. Box 217, Enschede, 7500 AE, The Netherlands.

²School of Mathematics and Statistics, University College Dublin, Belfield, Dublin 4, Ireland.

³Gran Sasso Science Institute, Viale Francesco Crispi, 7, L’Aquila, 67100, Italy.

⁴Max Planck Institute for Dynamics and Self-Organisation, Am Faßberg 17, Göttingen, 37077, Germany.

⁵Department of Modern Mechanics, University of Science and Technology of China, Hefei, 230027, China.

*Corresponding author(s). E-mail(s): e.bellincioni@utwente.nl;
k.zhong@utwente.nl; d.lohse@utwente.nl;

†These authors contributed equally to this work.

Abstract

Melting is omnipresent in nature and technology, with applications ranging from metallurgy [1–3], biology [4, 5], food science [6, 7], and latent thermal energy storage [8–10] to oceanography, geophysics, and climate science [11–25], and occurring on all scales from sub-millimeter to global scales. The key objective is to understand the rate at which an object melts as a function of its size and of the ambient conditions. To achieve this it is important to be able to extrapolate from small scale experiments and observations to large or even global scales. This is done by scaling laws. However, these are only meaningful if there is no transition from one scaling relation to another one. Here we show, however, that for both fixed and freely-advectioned melting objects immersed in a turbulent flow

a melting transition does exist, namely from slow melting at the small scales to fast melting at the large scales. We do so by controlled melting experiments and corresponding direct numerical simulations, covering four orders of magnitude in scale. The transition corresponds to the transition from a laminar-type boundary layer around the melting object to a turbulent-type boundary layer, i.e., from so-called classical turbulence to ultimate turbulence, with its enhanced transport properties [26–29]. Our results thus provide a quantitative understanding of the flow physics of the melting process and thereby enable a better extrapolation and prediction of melt rates on large scales such as relevant in geophysics, oceanography, and climate science [11–15, 19, 23–25, 30, 31].

The melting of icebergs or glacial ice into the ocean is not understood on a quantitative level. Such an understanding, however, is essential for reliable ocean and climate models and to predict the rise of the sea level. Present model predictions for the melting of ice into the ocean are often off by an order of magnitude or even more as compared to recent field measurements [16–18], different models give quite different results [19], and basal glacier melting into the ocean plays a much more prominent role than previously thought [20, 21]. The lack of understanding is on a fundamental level and one of the grand challenges in environmental fluid dynamics [22]; ice melting is a highly complex multi-scale, multi-physics problem, with multi-way coupling and memory effects. What considerably contributes to the complexity is that, in general, flow is turbulent around the melting ice, which in itself is already a multi-scale phenomenon.

A fundamental understanding of melting processes in turbulent flow is hugely relevant also in various other processes in nature and technology, ranging from metallurgy [1, 3], food science [6, 7], and—in the context of the energy transition—latent thermal energy storage with phase-change materials (PCMs) [8–10]. The latter is receiving recent industrial interest as it allows for the temporal mismatch between energy demand and supply to be mitigated, e.g. enabling the storage of the highly fluctuating solar or wind power in latent heat, and its later release when needed.

The main objective of fundamental research on melting in turbulent flow must be a quantitative prediction of the melt rates as function of the size of the melting object, both for fixed and for freely-advection objects. This prediction is often sought for in the form of scaling laws, which are based on controlled experiments and observations on small scales and then extrapolated to much larger systems. However, such extrapolations only make sense if there are no transitions from one scaling relation to another one. Turbulent flows, however, can show transitions between different turbulent states. For example, in thermally driven turbulence, beyond a certain range of driving strengths the system undergoes a transition from classical turbulence, where the boundary layers are of laminar type, to so-called ultimate turbulence, where the boundary layers become turbulent, leading to enhanced heat transfer [26, 28, 29]. For melting problems, such a transition would imply much larger melt rates above the transition. Indeed, the pioneering work by Machicoane *et al.* [32] on melting ice in turbulent flow identified a strong dependence of the melt rate on the degree of turbulence which corresponds to what we call “ultimate melting”.

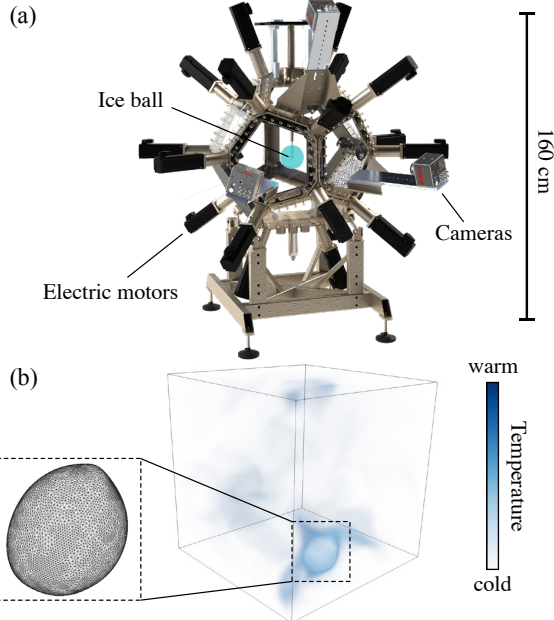


Fig. 1 Present experimental and numerical setups (a) Experimental setup: twenty independently-controlled electric motors mounted on the vertices of a ≈ 210 L dodecahedral water tank drive propellers to generate HIT in the tank center. (b) Volume contours of instantaneous temperature in our present DNS at $Re_\lambda \approx 50$, $Re_{D_0} \approx 80$ for a Lagrangian ball at 50% of its initial volume. The melting ball is represented by an immersed boundary [34], as visualized in the left panel.

However, to actually observe the transitions from one regime to another one, i.e., from slower melt rates to faster ones, is intrinsically difficult, as many orders of magnitude must be covered to reliably identify the transition. In this study we achieve this anyhow and cover four orders of magnitude in the size of the melting object, namely by combining experiments of melting ice blocks of various sizes in statistically stationary, homogeneous, isotropic turbulent flows of different strengths with direct numerical simulations of melting objects in corresponding turbulent flows and with several reanalysed data sets from the literature [32, 33]. In this sense our study can be seen as a meta-study: indeed, by this combination we do observe a clear transition between two quite different melting regimes, namely from slow or “classical melting” on the small scales, to fast or “ultimate melting” on the large scales. This transition is due to a transition in the boundary layer around the melting object, namely from a laminar type boundary layer—allowing only for weak heat transport—to a turbulent boundary layer—with much enhanced heat transport. This transition occurs in the range of shear Reynolds numbers being of the order of one hundred, as expected from the analogous transition in wall-bounded shear flows and thermally driven turbulence (in so-called Rayleigh–Bénard convection) [28, 29].

We perform experiments and simulations of ice balls melting in homogeneous isotropic turbulence, see figure 1. Sample movies visualizing the melting process in both our experiments and DNS are available as Supplementary Information. The details

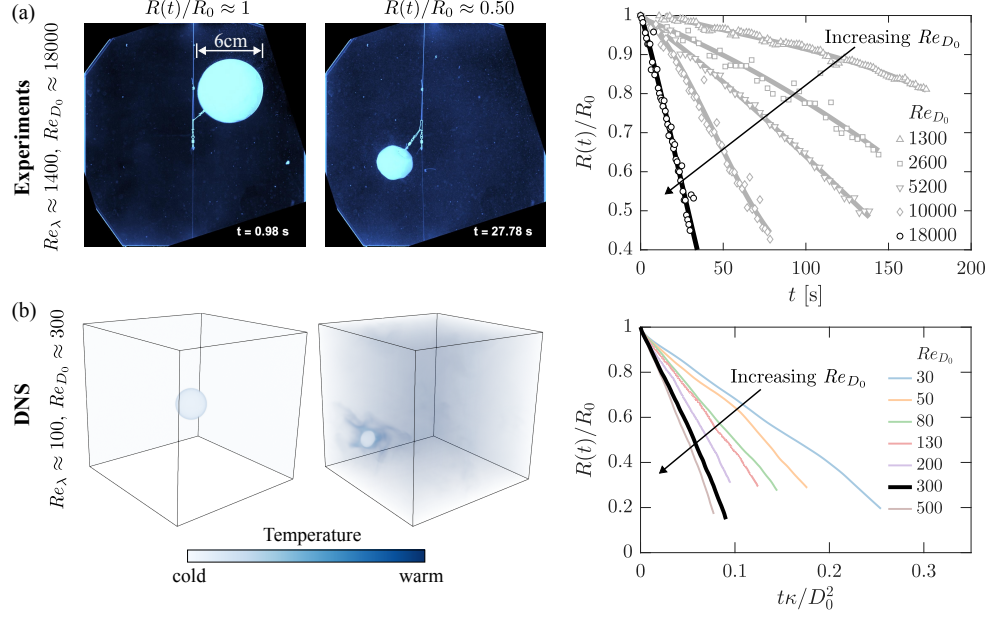


Fig. 2 Reynolds number controls melting rate of ice balls in both experiments and DNS
 Snapshots of a freely-ad advected melting ice ball at two different times at fixed Re_λ and fixed Re_{D_0} (as noted) and temporal evolution of the volume-equivalent radius for various Re_{D_0} . The dark curve corresponds to the case shown in the two left panels. (a) Experimental results (b) DNS results.

of both the experiments and DNSs can be found in [Methods](#). We call balls that are fixed in space Eulerian, and balls that are advected by the turbulent flow Lagrangian. The main dimensionless control parameters of both experiments and DNSs are the Taylor–Reynolds number of the flow $Re_\lambda \equiv \sqrt{15u_{\text{rms}}^4}/(\varepsilon\nu)$, with u_{rms} the root-mean-square of the velocity's fluctuations, ε the turbulent dissipation rate, ν the water's kinematic viscosity (which depends on temperature), and the initial ice ball Reynolds number $Re_{D_0} \equiv \mathcal{U}_{D_0} D_0/\nu$, where $\mathcal{U}_{D_0} \equiv (\varepsilon D_0)^{1/3}$ is the characteristic velocity of the turbulent flow at scale D_0 (the initial diameter of the ice ball). Further dimensionless control parameters of the system are the Prandtl number $Pr \equiv \nu/\kappa$, where κ is the thermal diffusivity of water (which depends on temperature), and the Stefan number $Ste \equiv c_{p,w} \Delta T_{\text{water}}/\mathcal{L}$, where \mathcal{L} is the latent heat of the ice, $c_{p,w}$ the specific heat of the water, and ΔT_{water} the temperature of the surrounding water above the melting temperature.

Figure 2a shows two snapshots of a melting ice ball for the Lagrangian case for very strong turbulence ($Re_\lambda \approx 1400$) and an initial ice ball Reynolds number $Re_{D_0} \approx 18000$. Figure 2a, right, also displays the temporal evolution of the volume-equivalent radius $R(t)$ of the ice ball (relative to its initial size R_0) for that case $Re_{D_0} \approx 18000$ (dark curve) and various other cases with smaller Re_{D_0} (light grey curves), for which the ice balls obviously melt more slowly. The analogous plots for DNS results are shown in figure 2b, though for a case of much weaker turbulence ($Re_\lambda \approx 100$; the largest Re_λ available from DNS is about 200) and with much smaller $Re_{D_0} \approx 300$.

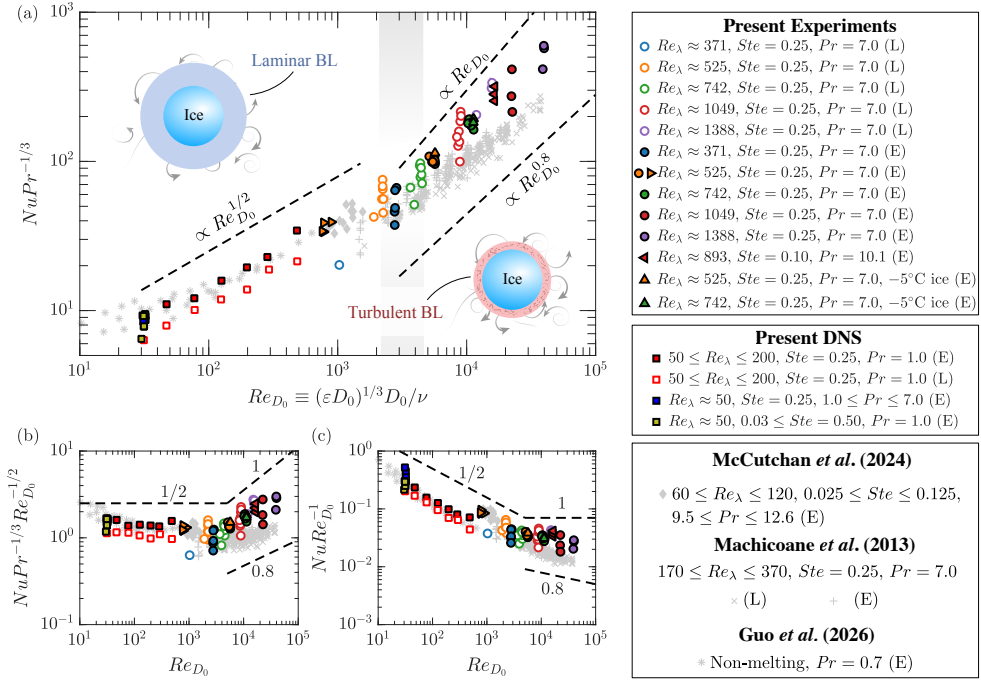


Fig. 3 A scaling transition from slow to fast melting (a) Nusselt number compensated by $Pr^{1/3}$ for all the presently considered experiments and DNS and data from the literature [32, 33, 35]. The dashed lines indicate $Nu \propto Re_{D_0}^{1/2}$, $Nu \propto Re_{D_0}^{0.8}$ and $Nu \propto Re_{D_0}$ scaling relations. The symbol legend indicates the Re_λ considered, Stefan number Ste , Prandtl number Pr , and whether Eulerian (E) or Lagrangian (L) melting is considered. The grey-shaded region indicates a range where the laminar-to-turbulent boundary-layer transition takes place. In the two sketches, the boundary-layer thickness is not to scale. (b) Data in (a) compensated by $Re_{D_0}^{-1/2}Pr^{1/3}$ to highlight the laminar boundary-layer scaling for $Re_{D_0} \lesssim 4000$. (c) Data in (a) compensated by Re_{D_0} highlighting the ultimate regime scaling. The dashed lines in (b,c) indicate $Nu \propto Re_{D_0}^{1/2}$, $Nu \propto Re_{D_0}$, $Nu \propto Re_{D_0}^{0.8}$ scalings.

Out of such temporal evolutions of the melting ice balls (either experimental or numerical) we can extract the mean melt rate $\langle \dot{R} \rangle$ (the average is over time) and its dependence on the control parameters. To allow for comparison between different experiments and simulations, the melt rate is expressed in dimensionless form as the Nusselt number Nu , which is the dimensionless heat transfer from the water towards the ice (see [Methods](#) for a detailed derivation)

$$Nu \approx -\frac{\rho_{\text{ice}}}{\rho_{\text{water}}} \frac{Pr}{Ste} \frac{\langle \dot{R} \rangle D_0}{\nu} \quad (1)$$

where $\rho_{\text{ice}}/\rho_{\text{water}} \approx 0.9$ is the ice-to-water density ratio.

The results for Nu (compensated by $Pr^{1/3}$ for reasons to be explained later) vs Re_{D_0} are shown in figure 3. The plot also contains (re-analysed) experimental data of Machicoane *et al.* [32], McCutchan *et al.* [33] (who varied Pr and Ste), and Guo *et al.*

[35] (for heat transfer without melting). In the melting experiments, Re_{D_0} varies by nearly two orders of magnitude, revealing a nearly linear dependence $Nu \propto Re_{D_0}^\gamma$ [32] with $0.8 \leq \gamma \leq 1.0$. The numerical data in the plot reflect the considerable lower Reynolds numbers ($Re_{D_0} < 700$), but note that the experimental and numerical data sets nearly overlap and show good agreement in the overall trend. From the experimental data, we cannot detect differences between the Eulerian and the Lagrangian cases; they are of similar magnitude as differences between repeated experiments for the same control parameters. The DNS data are more precise, and we can conclude that Eulerian melting is slightly faster than Lagrangian melting, due to the larger shear rates achieved along the melting object in the Eulerian case. But most importantly in the context of this work, four orders of magnitude in Re_{D_0} are covered. This large range enables us to now clearly identify the existence of two different scaling regimes and the transition in between them, namely the above mentioned large Re_{D_0} regime with $Nu \propto Re_{D_0}^\gamma$ with $0.8 \leq \gamma \leq 1.0$ above the transition and a small Re_{D_0} regime with $Nu \propto Re_{D_0}^{1/2}$ below the transition.

This latter scaling relation can be directly understood from the Prandtl–Blasius–Pohlhausen theory [29, 36, 37] of heat transfer through a laminar-type thermal boundary layer over a hot or cold plate, $Nu \propto Re^{1/2} Pr^{1/3}$ for $Pr > 1$. This Pr -dependence of $Nu \propto Pr^{1/3}$ is the reason why we compensate Nu with $Pr^{1/3}$ in figure 3, in order to be able to compare results for different Pr . For increasing Reynolds numbers, however, at some point the thermal boundary layer around the melting object can no longer be of laminar type, and undergoes a transition to a turbulent boundary layer of Prandtl–von Kármán type [29, 36, 37]. The nature of this transition is of non-normal, nonlinear type [27], i.e., there is no precise critical shear Reynolds number Re_s , but a range of Re_s where the transition can happen, depending on the noise present in the system. For the canonical flat-plate boundary-layer one typically has $100 \leq Re_s \leq 500$ [29], whereas in our present case, the transition we observe occurs around $Re_{D_0} \approx 4000$, implying a shear Reynolds number of $Re_s \approx Re_{D_0}^{1/2} \approx 60$. The reasons why the observed onset of the transition is slightly earlier as compared to the classical flat-plate estimate are manifold: Besides inherent differences in geometry, well-understood effects which are known to promote boundary-layer receptivity (i.e. its sensitivity to noise) include [36, 38, 39]: surface roughness [40] (see for instance the classical textbook example of the dimpled golf ball to trigger early transition), freestream turbulence [41], unsteady flow effects [42], and 3D-effects or non-parallel flows [43, 44]. All the effects mentioned are expected to be present in our melting configuration and account for the early $Re_s \approx 60$ transition onset.

Beyond the transition, i.e., for the case of a turbulent boundary layer around the melting object, the heat transfer scales as [29, 45]

$$Nu \propto Re \mathcal{L}(Re) \quad (2)$$

for $Pr > 1$, as relevant for water. Here Re is a system-size-scaled Reynolds number which here we identify with the Reynolds number Re_{D_0} of the melting object and $\mathcal{L}(Re)$ denotes logarithmic corrections with respect to Re . Over the range of relevant Reynolds numbers, relation (2) with its logarithmic correction is indistinguishable from

an effective power law [45] $Nu \propto Re_{D_0}^{0.8}$, which is a common engineering correlation for turbulent heat transfer systems [46, 47] and is consistent with the observed data in figure 3.

We note that the observed melting transition is analogous to the experimentally observed transition in heat transfer around a heated ball in air flows [48]. Also in that case an increase in the Nusselt number beyond a certain Reynolds number range is achieved, analogous to the drag crisis for the drag force on the sphere.

There is yet another interesting aspect in the data of figure 3: while the melting rate clearly depends on Re_{D_0} , it hardly does so on the Taylor–Reynolds number Re_λ of the surrounding flow. For example, the green circles in figure 3 share the same Re_λ , but differ significantly in Re_{D_0} and Nu . Whereas Re_λ characterises the full range of large- and small-eddies in the system, Re_{D_0} characterises only the range from the melting object size to the smallest eddies. The fact that melting depends strongly on Re_{D_0} but not on Re_λ , then, implies that only eddies of the size of the melting object and smaller are responsible for the melting process. The situation is similar as for droplets in turbulent flow, which according to the Kolmogorov–Hinze theory [49] become fragmented by eddies of the size of the droplet and smaller ones, but not by larger ones.

In summary, by a meta-study of melting experiments and direct numerical simulations in turbulent flow over a very large range of four orders of magnitude in the Reynolds number of the melting object we have observed the transition from classical melting with $Nu \propto Re_{D_0}^{1/2}$ to ultimate melting with $Nu \propto Re_{D_0}^\gamma$ for $0.8 \leq \gamma \leq 1$, and interpret it as the transition from a laminar-type boundary layer to a turbulent boundary layer. The existence of this universal fluid dynamics transition in the melting process has profound implications for climate modelling: current parametrizations assume a single scaling relationship across all scales, whereas we show that the dependency on the Reynolds number must not be underestimated. Although the gap from laboratory experiments to geophysical scales is still far from being filled, identifying regime transitions and providing a sound understanding of the physics are key in safely extrapolating results of experiments from small scales to large ones—an ability which is greatly needed in the geophysical and industrial context.

Methods

Derivation of relation between melt rate and Nusselt number

The starting point for the connection of $\langle \dot{R} \rangle$ and Nu is the integrated heat balance at the interface, given by the Stefan condition [50–53]

$$-\mathcal{L}\rho_{\text{ice}}\langle \dot{R} \rangle = \lambda_{\text{water}} \left\langle \frac{\partial T}{\partial n} \right\rangle_{\text{water}} - \lambda_{\text{ice}} \left\langle \frac{\partial T}{\partial n} \right\rangle_{\text{ice}}. \quad (3)$$

Here $\partial/\partial n \equiv \hat{\mathbf{n}} \cdot \nabla$ denotes the gradient in the local interface-normal direction $\hat{\mathbf{n}}$, which points from the ice phase to the water phase and is evaluated at either the water-side of the interface ($|_{\text{water}}$) or the ice-side ($|_{\text{ice}}$), and $\lambda \equiv \rho c_p \kappa$ is the thermal conductivity of the respective phases. Here, the average $\langle \cdot \rangle$ refers to an average over

the solid surface and over the melting duration. With the dimensionless heat transfer coefficients for the water-side convection, which is the Nusselt number

$$Nu \equiv \left\langle \frac{\partial T}{\partial n} \right\rangle \Big|_{\text{water}} \frac{D_0}{\Delta T_{\text{water}}}, \quad (4)$$

and the ice-side conduction, which is the Biot number

$$Bi \equiv \left\langle \frac{\partial T}{\partial n} \right\rangle \Big|_{\text{ice}} \frac{D_0}{\Delta T_{\text{ice}}}, \quad (5)$$

we obtain the dimensionless form of the Stefan condition (3), namely

$$-\frac{\rho_{\text{ice}}}{\rho_{\text{water}}} \frac{Pr}{Ste} \frac{\langle \dot{R} \rangle D_0}{\nu} = Nu - \frac{\lambda_{\text{ice}}}{\lambda_{\text{water}}} \frac{\Delta T_{\text{ice}}}{\Delta T_{\text{water}}} Bi. \quad (6)$$

This equation expresses a balance between the dimensionless melt rate $\langle \dot{R} \rangle D_0 / \nu$ and the sensible heat transfers on the water and ice side, given by the convective (water-side) heat transfer coefficient Nu , and the solid-side heat transfer coefficient Bi .

The balance is typically simplified by recognizing that fluid convection can provide far more efficient heat transfer than conduction through a solid, such that $Nu \gg Bi$ [54]. Moreover, $\Delta T_{\text{ice}} / \Delta T_{\text{water}}$ and $\lambda_{\text{ice}} / \lambda_{\text{water}}$ are both $\mathcal{O}(1)$ prefactors in front of Bi so the last term on the right-hand side of (6) can be neglected. This then yields the desired relation between the measured dimensional melt rate $\langle \dot{R} \rangle$ of the ice block and the Nusselt number, namely eq. (1).

Experimental setup

Our experiments were carried out in a water tank in the shape of a regular dodecahedron, with the side measuring 30 cm. The volume of the temperature-controlled water in the tank is approximately 210 L. At each of the 20 vertices of the dodecahedron 3D-printed toroidal propellers connected to electric motors drive the flow, each one with a maximum power of ≈ 1 kW. With them we generate (approximately) homogeneous, isotropic, and statistically stationary turbulence, whose strength is quantified by its Taylor–Reynolds number Re_λ . We then put ice balls of three different diameters (3 cm, 6 cm, and 12 cm, corresponding to volumes of 0.01 L, 0.11 L, and 0.90 L) into the flow, either in an Eulerian way (i.e., at fixed position in the center of the flow) or in a (quasi)-Lagrangian way (i.e., by letting them freely advect in the bulk of the flow, but limiting it to the center where the flow is approximately HIT and furthermore preventing collisions with the propellers and the walls by loosely holding them with interconnected wires). For the Eulerian case, the size of the melting ice balls was measured by a single Nikon D850 camera with a Zeiss 100 mm objective (resolution $45 \mu\text{m px}^{-1}$, 2 fps). For the Lagrangian case, we measured with three high-speed cameras (Photron AX200 with Nikon AF Nikkor 50 mm f/1.8D objective, resulting in a resolution of $\approx 175 \mu\text{m px}^{-1}$, operating at 31.25 fps), mounted on three adjacent windows of the dodecahedron.

Experimentally, we measure the root-mean-square of the velocity fluctuations u_{rms} with Lagrangian doppler velocimetry (LDV), and apply the method described in van Buuren et al. [55] to obtain the dissipation rate ε .

More details on the experiments, including details on the balls' 3D spherical fit method and detailed measurements of the turbulence in the tank, will be provided in a forthcoming publication.

Numerical setup

Our direct numerical simulations (DNSs) were conducted by solving the underlying incompressible Navier–Stokes equations for the velocity field, together with the advection–diffusion equation for the temperature field. The computational domain is a cube with periodic boundary conditions applied in all three directions. Homogeneous isotropic turbulent flow conditions are sustained through a large-scale forcing which acts on the momentum field [56]. To facilitate melting, we use the method detailed in Zhong *et al.* [34] which employs an immersed boundary framework to represent the melting ice and enforces the correct boundary conditions at the melting interface (i.e. the Stefan boundary condition [52]). The additional novelty of this framework is its ability to solve the Lagrangian melting case, where both the dynamics of the melting ice and fluid flow are two-way coupled and solved in tandem, allowing for the melting ice to be freely advected by the flow. Precise details on the implementation of the numerical method and its validation can be found in ref. [34]. Further details on the full set of simulation runs presented and their employed and achieved parameter choices will be provided in a forthcoming publication.

Supplementary Information. This work has Supplementary Videos: two experiments ($Re_{D_0} \approx 18000$, $Re_\lambda \approx 1400$; and $Re_{D_0} \approx 2600$, $Re_\lambda \approx 500$) and two DNS ($Re_{D_0} \approx 300$, $Re_\lambda \approx 100$; and $Re_{D_0} \approx 80$, $Re_\lambda \approx 50$)

Acknowledgements. We thank Gert-Wim Bruggert, Martin Bos, and Thomas Zijlstra for technical support. We thank Romain Volk and Nathanaël Machicoane for making the raw data of ref. [32] available to us.

Declarations

- *Funding* This work was financially supported by the European Union (ERC, MeltDyn, 101040254 and ERC, MultiMelt, 101094492).
- *HPC* This work was carried out on the Dutch national e-infrastructure with the support of SURF Cooperative. We acknowledge the EuroHPC Joint Undertaking for awarding the project EHPC-REG-2023R03-178 access to the EuroHPC supercomputer Discoverer, hosted by Sofia Tech Park (Bulgaria). We also acknowledge the EuroHPC Joint Undertaking for awarding the project ID EHPC-EXT-2024E02-122 access to the MareNostrum V system hosted by the Barcelona Supercomputing Center (BSC), Spain.
- *Authors contributions* E.B., Y.Z., and S.G.H. performed the experiments; K.Z., C.J.H., and R.V. performed the DNS; D.L. conceived the idea. All authors edited the manuscript.

- The authors declare no competing interests.

References

- [1] Wang, Y., Cao, L., Cheng, Z., Blanpain, B., Guo, M.: Mathematical methodology and metallurgical application of turbulence modelling: A review. *Metals* **11**(8) (2021)
- [2] Chakraborty, N.: The effects of turbulence on molten pool transport during melting and solidification processes in continuous conduction mode laser welding of copper–nickel dissimilar couple. *Appl. Therm. Eng.* **29**(17–18), 3618–3631 (2009)
- [3] Aboutalebi, M.R., Hasan, M., Guthrie, R.: Coupled turbulent flow, heat, and solute transport in continuous casting processes. *Metall. Mater. Trans. b* **26**(4), 731–744 (1995)
- [4] Farrant, J.: Mechanism of cell damage during freezing and thawing and its prevention. *Nature* **205**(4978), 1284–1287 (1965)
- [5] Uhrig, M., Ezquer, F., Ezquer, M.: Improving cell recovery: freezing and thawing optimization of induced pluripotent stem cells. *Cells* **11**(5), 799 (2022)
- [6] Mathijssen, A.J., Lisicki, M., Prakash, V.N., Mossige, E.J.: Culinary fluid mechanics and other currents in food science. *Rev. Mod. Phys.* **95**(2), 025004 (2023)
- [7] Norton, T., Sun, D.-W.: Computational fluid dynamics (CFD)–an effective and efficient design and analysis tool for the food industry: A review. *Trends Food Sci. Technol.* **17**(11), 600–620 (2006)
- [8] Vogel, J., Thess, A.: Validation of a numerical model with a benchmark experiment for melting governed by natural convection in latent thermal energy storage. *Appl. Thermal Eng.* **148**, 147–159 (2019)
- [9] Li, Q., Li, C., Du, Z., Jiang, F., Ding, Y.: A review of performance investigation and enhancement of shell and tube thermal energy storage device containing molten salt based phase change materials for medium and high temperature applications. *Appl. Energy* **255**, 113806 (2019)
- [10] Jouhara, H., Żabieńska-Góra, A., Khordehgah, N., Ahmad, D., Lipinski, T.: Latent thermal energy storage technologies and applications: A review. *Int. J. Thermofluids* **5**, 100039 (2020)
- [11] Hewitt, I.J.: Subglacial plumes. *Annu. Rev. Fluid Mech.* **52**, 145–169 (2020)
- [12] Straneo, F., Cenedese, C.: The dynamics of greenland’s glacial fjords and their role in climate. *Annu. Rev. Marine Sci.* **7**, 89–112 (2015)

- [13] Cenedese, C., Straneo, F.: Icebergs melting. *Annu. Rev. Fluid Mech.* **55**(1), 377–402 (2023)
- [14] Pritchard, H., Ligtenberg, S.R., Fricker, H.A., Vaughan, D.G., Broeke, M.R., Padman, L.: Antarctic ice-sheet loss driven by basal melting of ice shelves. *Nature* **484**(7395), 502–505 (2012)
- [15] Shepherd, A., Ivins, E.R., A, G., Barletta, V.R., Bentley, M.J., Bettadpur, S., Briggs, K.H., Bromwich, D.H., Forsberg, R., Galin, N., *et al.*: A reconciled estimate of ice-sheet mass balance. *Science* **338**(6111), 1183–1189 (2012)
- [16] Stroeve, J., Holland, M.M., Meier, W., Scambos, T., Serreze, M.: Arctic sea ice decline: Faster than forecast. *Geophys. Res. Lett.* **34**(9), 09501 (2007)
- [17] Sutherland, D., Jackson, R.H., Kienholz, C., Amundson, J.M., Dryer, W., Duncan, D., Eidam, E., Motyka, R., Nash, J.: Direct observations of submarine melt and subsurface geometry at a tidewater glacier. *Science* **365**(6451), 369–374 (2019)
- [18] Buzzard, S.: The surface hydrology of Antarctica’s floating ice. *Phys. Today* **75**(1), 28–35 (2022)
- [19] Malyarenko, A., Wells, A.J., Langhorne, P.J., Robinson, N.J., Williams, M.J., Nicholls, K.W.: A synthesis of thermodynamic ablation at ice–ocean interfaces from theory, observations and models. *Ocean Modell.* **154**, 101692 (2020)
- [20] Young, T.J., Christoffersen, P., Bougamont, M., Tulaczyk, S.M., Hubbard, B., Mankoff, K.D., Nicholls, K.W., Stewart, C.L.: Rapid basal melting of the Greenland Ice Sheet from surface meltwater drainage. *Proc. Natl. Acad. Sci.* **119**(10), 2116036119 (2022)
- [21] Larter, R.D.: Basal melting, roughness and structural integrity of ice shelves. *Geophys. Res. Lett.* **49**, 2021–097421 (2022)
- [22] Dauxois, T., Peacock, T., Bauer, P., Caulfield, C.P., Cenedese, C., Gorlé, C., Haller, G., Ivey, G.N., Linden, P.F., Meiburg, E., Pinardi, N., Vriend, N.M., Woods, A.W.: Confronting grand challenges in environmental fluid mechanics. *Phys. Rev. Fluids* **6**(2), 020501 (2021)
- [23] Noël, B., Van Wessem, J.M., Wouters, B., Trusel, L., Lhermitte, S., Van Den Broeke, M.R.: Higher antarctic ice sheet accumulation and surface melt rates revealed at 2 km resolution. *Nature Commun.* **14**(1), 7949 (2023)
- [24] Hanna, E., Topál, D., Box, J.E., Buzzard, S., Christie, F.D., Hvidberg, C., Morlighem, M., De Santis, L., Silvano, A., Colleoni, F., *et al.*: Short-and long-term variability of the antarctic and greenland ice sheets. *Nature Reviews Earth & Environment* **5**(3), 193–210 (2024)

- [25] Lucas, N.S., Brearley, J.A., Hendry, K.R., Spira, T., Braakmann-Folgmann, A., Abrahamsen, E.P., Meredith, M.P., Tarling, G.A.: Giant iceberg meltwater increases upper-ocean stratification and vertical mixing. *Nature Geoscience*, 1–8 (2025)
- [26] Kraichnan, R.H.: Turbulent thermal convection at arbitrary Prandtl number. *Phys. Fluids* **5**, 1374–1389 (1962)
- [27] Avila, M., Barkley, D., Hof, B.: Transition to turbulence in pipe flow. *Annu. Rev. Fluid Mech.* **55**, 575–602 (2023)
- [28] Lohse, D., Shishkina, O.: Ultimate turbulent thermal convection. *Phys. Today* **76**(11), 26–32 (2023)
- [29] Lohse, D., Shishkina, O.: Ultimate Rayleigh–Bénard turbulence. *Rev. Mod. Phys.* **96**, 035001 (2024)
- [30] Hester, E.W., McConnochie, C.D., Cenedese, C., Coustou, L.-A., Vasil, G.: Aspect ratio affects iceberg melting. *Phys. Rev. Fluids* **6**(2), 023802 (2021)
- [31] Wells, A.J., Worster, M.G.: A geophysical-scale model of vertical natural convection boundary layers. *J. Fluid Mech.* **609**, 111–137 (2008)
- [32] Machicoane, N., Bonaventure, J., Volk, R.: Melting dynamics of large ice balls in a turbulent swirling flow. *Phys. Fluids* **25**(12), 125101 (2013)
- [33] McCutchan, A.L., Meyer, C.R., Johnson, B.A.: Enhancement of ice melting in isotropic turbulence. *Phys. Rev. Fluids* **9**(7), 074601 (2024)
- [34] Zhong, K., Howland, C.J., Lohse, D., Verzicco, R.: A front-tracking immersed-boundary framework for simulating Lagrangian melting problems. *J. Comput. Phys.* **525**, 113762 (2025)
- [35] Guo, H., Zhang, X., Feng, L., Wu, Y., Wu, Y.: Experimental Nusselt number correlations for heat transfer of a single spherical particle in turbulent flow. *Int. J. Heat Mass Transf.* **256**, 127939 (2026)
- [36] Schlichting, H.: *Boundary Layer Theory*, 7th edn. McGraw Hill, New York (1979)
- [37] Ahlers, G., Grossmann, S., Lohse, D.: Heat transfer and large scale dynamics in turbulent Rayleigh–Bénard convection. *Rev. Mod. Phys.* **81**, 503 (2009)
- [38] Schmid, P.J., Henningson, D.S.: *Stability and Transition in Shear Flows*, 1st edn. Springer, New York (2001)
- [39] Drazin, P.G., Reid, W.H.: *Hydrodynamic Stability*, 2nd edn. Cambridge University Press, Cambridge (2004)

- [40] Dryden, H.L.: Review of published data on the effect of roughness on transition from laminar to turbulent flow. *J. Aero. Sci.* **20**(7), 477–482 (1953)
- [41] Kendall, J.: Boundary layer receptivity to freestream turbulence. *AIAA Paper*, 90–1504 (1990)
- [42] Obremski, H.J., Fejer, A.A.: Transition in oscillating boundary layer flows. *J. Fluid Mech.* **29**(1), 93–111 (1967)
- [43] Klebanoff, P.S., Tidstrom, K.D., Sargent, L.M.: The three-dimensional nature of boundary-layer instability. *J. Fluid Mech.* **12**(1), 1–34 (1962)
- [44] Saric, W.S., Nayfeh, A.H.: Nonparallel stability of boundary-layer flows. *Phys. Fluids* **18**(8), 945–950 (1975)
- [45] Grossmann, S., Lohse, D.: Multiple scaling in the ultimate regime of thermal convection. *Phys. Fluids* **23**, 045108 (2011)
- [46] Bejan, A.: *Heat Transfer*. John Wiley and Sons. Inc., New York (1993)
- [47] Kays, W.M., Crawford, M.E.: *Convective Heat and Mass Transfer*, 3rd edn. McGraw-Hill, New York (1993)
- [48] Will, J.B., Kruyt, N.P., Venner, C.H.: An experimental study of forced convective heat transfer from smooth, solid spheres. *Int. J. Heat Mass Transf.* **109**, 1059–1067 (2017)
- [49] Ni, R.: Deformation and breakup of bubbles and drops in turbulence. *Annu. Rev. Fluid Mech.* **56**(1), 319–347 (2024)
- [50] Carslaw, H.S., Jaeger, J.C.: *Conduction of Heat in Solids*. Oxford University Press, Oxford (1959)
- [51] Alexiades, V., Solomon, A.D.: *Mathematical Modeling of Melting and Freezing Processes*. Taylor & Francis, London (1993). <https://doi.org/10.1201/9780203749449>
- [52] Worster, M.G.: Solidification of fluids. In: *Perspectives in Fluid Dynamics*, pp. 393–446. Cambridge University Press, Cambridge (2000)
- [53] Davis, S.H.: *Theory of Solidification*. Cambridge University Press, Cambridge (2004)
- [54] Dinniman, M.S., Asay-Davis, X.S., Galton-Fenzi, B.K., Holland, P.R., Jenkins, A., Timmermann, R.: Modeling ice shelf/ocean interaction in antarctica: A review. *Oceanography* **29**(4), 144–153 (2016) <https://doi.org/10.5670/oceanog.2016.106>

- [55] van Buuren, D., van Gils, D.P.M., Bruggert, G.-W., Krug, D.: TWISTER (Twente water injection system for turbulence experimental research): a jet array in the Twente water tunnel for generating strong turbulence using four-dimensional gradient noise. *Exp Fluids* **66**(10), 184 (2025)
- [56] Eswaran, V., Pope, S.B.: An examination of forcing in direct numerical simulations of turbulence. *Comput. Fluids* **16**(3), 257–278 (1988)